Magnetoresistance of a single polycrystalline nickel nanowire

S. N. Kozlov, O. V. Skryabina, S. V. Egorov, I. A. Golovchanskiy (iD), A. A. Klimenko, K. S. Napolskii (iD), and V. S. Stolyarov (iD)

View Online   Export Citation   CrossMark

ARTICLES YOU MAY BE INTERESTED IN

Frontiers of magnetic force microscopy
Journal of Applied Physics **125**, 060901 (2019); https://doi.org/10.1063/1.5050712

Tunable specific-loss power of magnetic nano-spheres in vortex state for high-efficiency hyperthermia bio-applications: A theoretical and simulation study
Journal of Applied Physics **125**, 063901 (2019); https://doi.org/10.1063/1.5055805

Interaction and transfer of charged particles from an alternating current glow discharge in liquids: Application to silver nanoparticle synthesis
Journal of Applied Physics **125**, 063303 (2019); https://doi.org/10.1063/1.5063872

Magnetoresistance of a single polycrystalline nickel nanowire

View Online   Export Citation   CrossMark

S. N. Kozlov,[1,2,a)] O. V. Skryabina,[2,3] S. V. Egorov,[3,4] I. A. Golovchanskiy,[2,5] (iD) A. A. Klimenko,[6,7] K. S. Napolskii,[6,8] (iD) and V. S. Stolyarov[2,9,b)] (iD)

AFFILIATIONS

[1]Fundamental Physical and Chemical Engineering Department, MSU, 119991 Moscow, Russia
[2]Moscow Institute of Physics and Technology, 141700 Dolgoprudny, Russia
[3]Institute of Solid State Physics RAS, 142432 Chernogolovka, Russia
[4]Russian Quantum Center, Skolkovo, 143025 Moscow, Russia
[5]The Laboratory of Superconducting Metamaterials, National University of Science and Technology MISIS, 119049 Moscow, Russia
[6]Department of Materials Science, MSU, 119991 Moscow, Russia
[7]Institute of Nanotechnology of Microelectronics RAS, 119991 Moscow, Russia
[8]Department of Chemistry, MSU, 119991 Moscow, Russia
[9]Solid State Physics Department, KFU, 420008 Kazan, Russia

[a)]**Electronic mail:** sergeikozlov24@yandex.ru
[b)]**Electronic mail:** vasiliy.stoliarov@gmail.com

ABSTRACT

We report the magnetoresistance study of an individual polycrystalline nickel nanowire at temperature $T = 10$ K. Transport measurements have indicated a large coercive field of the nanowire, justified by the polycrystalline structure of the studied sample, where both magnetocrystalline anisotropy of randomly oriented grains and effective uniaxial anisotropy at the grain boundaries enhance the coercive field. Magnetization reversal studied with micromagnetic simulations occurs via the curling mode when vortices are nucleated and propagate along the nanowire, and propagation is inhibited at grain boundaries. The applicability of micromagnetic simulations is confirmed by a good agreement between experimental and simulated magnetoresistance curves.

I. INTRODUCTION

Magnetic nanowires (NWs) are of great interest nowadays due to the progress in nanofabrication and a trend for miniaturization of electronic components. Ferromagnetic NWs exhibit unique magnetic properties that are very different from those of bulk ferromagnetic materials, thin films, and spherical particles. In addition, these properties can be tuned in wide ranges adjusting fabrication parameters of NWs.[1,2] Their possible applications are magnetic memory,[3,4] logic devices,[5] and signal processing devices[6] to flexible electronics[7] and acoustic sensors.[8] The application of the ferromagnetic nanowires has been boosted recently for superconducting electronic devices.[9–11] All these applications rely on the magnetic properties and the behavior of magnetization of nanowires.

Therefore, the characterization of properties of NWs, their reproducibility, and theoretical representation are crucial. Apart from practical applications, there is an interest in the ferromagnetic nanowires for fundamental research. NWs are regarded as a playground with magnetic topological defects, e.g., skyrmions[12] and Bloch points.[13]

Nickel nanowires are often of specific interest due to the smallest susceptibility among elemental ferromagnetic metals, and, correspondingly, lower magnetic fields required for operation. Commonly, magnetic and transport properties of nickel NWs have been studied on arrays of nanowires.[14–16] The employment of an array simplifies measurement due to easier sample handling and larger signals to acquire, yet introduces the averaging of recorded responses and also

unnecessary magnetostatic interaction between NWs.[17] More accurate studies of individual NWs require more sophisticated measurement techniques as SQUID[18] or MOKE.[17] Magnetoresistance (MR) has also become a useful method to study the magnetization reversal process in NWs due to its sensitivity to small changes in magnetization.[19,20] In particular, transport properties of a single-crystal nickel NW are reported in Refs. [21] and [22].

Hysteresis behavior and MR of ferromagnetic NWs can be considered analytically for the "ideally soft" NWs, where magnetic anisotropies are absent and material properties of NWs are constant throughout a sample.[23–25] Indeed, the only three competing fields for the "ideally soft" NW are the applied field, the exchange field, and the demagnetizing magnetostatic field, and the last field is determined by dimensions of a NW. MR of a polycrystalline NW is more complex and requires the consideration of a contribution of crystallographic misorientation of crystallites[1,20,26,27] and grain boundaries.[28,29]

In this work, we focus on magnetoresistance of individual polycrystalline nickel nanowire at a low temperature using magnetoresistance measurements and micromagnetic simulations. We show that behavior of MR is dominated by the polycrystalline morphology of the nanowire, by magnetocrystalline anisotropy of individual grains, and also by magnetic properties of grain boundaries. Micromagnetic representation of these contributions allowed us to reproduce accurately the experimental magnetoresistance curve.

II. FABRICATION AND MEASUREMENT DETAILS

One of the most accessible synthesis methods for polycrystalline[30,31] and single-crystalline[2,31] nickel nanowires is electrodeposition inside the anodic aluminium oxide (AAO) template. In this work, AAO templates with a pore diameter of 125 ± 25 nm were used. Nickel nanowires were grown by the templated electrodeposition technique using electrolyte containing 0.6M $NiSO_4$, 0.1M $NiCl_2$, and 0.3M H_3BO_3 at a deposition potential of 0.9 V versus Ag/AgCl. In order to extract nickel nanowires, the oxide matrix was selectively dissolved in oxidant-free alkaline solution (for more details, please refer to the supplementary materials in Ref. [32]). Transmission electron microscopy (TEM) and selected area electron diffraction (SAED) studies showed that Ni NWs are polycrystalline with the grain size of the order of the nanowire diameter [see Figs. 1(a) and 1(b)]. The length of some grains reaches 600–700 nm. Ni NWs are coated with native nickel oxide with a thickness of approximately 2–4 nm, which protect nanowires from further degradation.

The fabrication process[32] was followed by bonding individual NWs with niobium electrodes for transport measurements. Nanowires were placed on the Si/SiO_2 substrate and attached to niobium contacts by means of electron beam (e-beam) lithography, argon etching, RF-magnetron sputtering, and lift-off. A set of samples with similar geometrical parameters and measured characteristics was fabricated. In this work, we focus on the sample with the Ni NW diameter of 137 ± 5 nm and the width between voltage
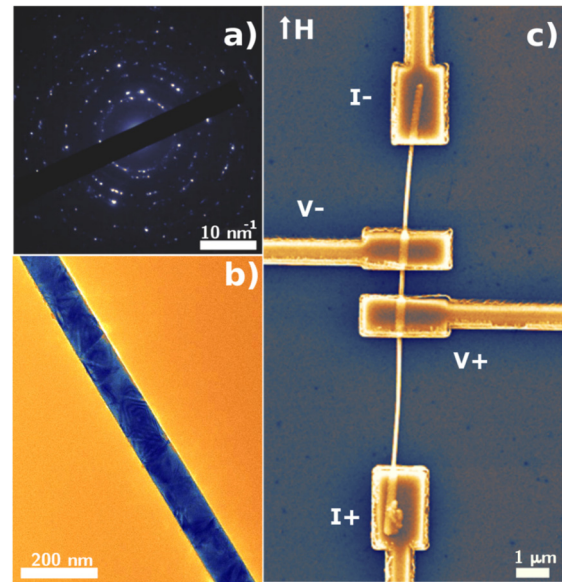

FIG. 1. SAED pattern (a) and TEM image (b) of the nickel nanowire that highlight its polycrystalline structure. (c) SEM image of the sample used for transport measurements.

contacts 800 nm. The scanning electron microscopy (SEM) image of the studied sample is shown in Fig. 1(c).

Transport properties of nickel nanowires were measured by the four-probe method in a He-4 cryostat equipped with a superconducting solenoid. The applied magnetic field was directed along the axis of the nanowire. The same experimental setup was used as in Ref. [32]. All measurement lines were equipped with low temperature RC filters. Magnetoresistance measurements were performed at 10 K, i.e., above the superconducting critical temperature of niobium, in order to exclude the influence of superconductivity of niobium contacts. To achieve a constant temperature above liquid helium temperature, the sample holder was equipped with a heater.

III. SIMULATION DETAILS

Micromagnetic simulations are shown to be useful for the simulation of magnetoresistance behavior of ferromagnetic nanowires.[33] The micromagnetic approach is based on solving the Landau-Lifshitz-Gilbert (LLG) equation which describes dynamics of local magnetization vector **M**. In terms of unit local magnetization vector $\mathbf{m} = \mathbf{M}/M_s$, where M_s is the saturation magnetization, the dynamics is given by

$$\frac{d\mathbf{m}}{dt} = \frac{\gamma}{1+\alpha^2}(\mathbf{m} \times \mathbf{H}_{eff} + \alpha\mathbf{m} \times \mathbf{m} \times \mathbf{H}_{eff}), \qquad (1)$$

where γ is the gyromagnetic ratio, α is the dimensionless Gilbert damping constant, and $\mathbf{H}_{eff}$ is the effective field which includes the demagnetization field $\mathbf{H}_d$, exchange field $\mathbf{H}_e$, magnetocrystalline anisotropy field $\mathbf{H}_a$, and external magnetic

field $\mathbf{H}$,

$$\mathbf{H}_{eff} = \mathbf{H}_d + \mathbf{H}_e + \mathbf{H}_a + \mathbf{H}. \qquad (2)$$

The numerical solution of the LLG equation was provided by the finite difference method[34] using MuMax3,[35] an open-source GPU-accelerated micromagnetic simulation program. The following parameters for micromagnetic simulations were used, typical for Ni: exchange constant $A = 1.05 \times 10^{11}$ J/m and tabulated saturation magnetization $M_s = 4.95 \times 10^5$ A/m (see Ref. 27), providing exchange length $l_e = \sqrt{2A/\mu_0 M_s^2} \simeq 8.3$ nm.

IV. RESULTS AND DISCUSSION

The MR curve R(H) indicates conventional longitudinal magnetoresistance (LMR).[36–38] The resistivity of a ferromagnet depends on the angle between applied current and local magnetization. For a mono-domain particle, resistivity is given by[39]

$$\rho(\phi) = \rho_o(1 + \beta \cos^2 \phi), \qquad (3)$$

where ρ_o is the resistivity of the demagnetized sample, ϕ is the angle between the applied current and magnetization vector, and β is the coefficient of anisotropic magnetoresistance. In the geometry of the present experiment where the magnetic field is aligned along the NW, the value $\cos \phi$ denotes the component of the unit magnetization vector on the axis of the NW m_x, and Eq. (3) can be rewritten as

$$\rho(m_x) = \rho_o(1 + \beta m_x^2). \qquad (4)$$

Therefore, the MR curve R(H) in Fig. 2 (dotted curve) follows hysteresis dependence of magnetization of the Ni NW in the aligned magnetic field: R(H) jumps up at the coercive field $H_c = \pm 76$ mT and depends on the magnetic field marginally at $H \gg H_c$. The jump of R(H) at H_c is about $0.02\,\Omega$. The
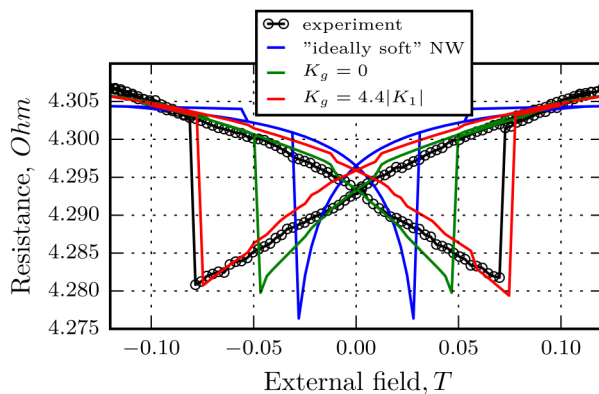
FIG. 2. Longitudinal magnetoresistance curves R(H). Open circles correspond to the experimental results. Theoretical fits obtained from the micromagnetic simulation are given by solid lines. Blue line denotes the MR for the "ideally soft" NW. Green line demonstrates the MR of polycrystalline NW with randomly oriented grains. Red line denotes the MR of polycrystalline NW with randomly oriented grains and effective uniaxial anisotropy at grain boundaries.

sample is characterized by resistivity $\rho = 7.7\,\mu\Omega$ cm, which is in the range of typical values achieved earlier for nickel nanowires at helium temperature.[9,21,22,40] The morphology of such a low dimensional object as a nanowire plays a crucial role because resistivity is mostly defined by scattering at nanowire's surface and defects. For Ni NWs, resistivity typically varies from $\simeq 24\,\mu\Omega$ cm[21,22,41] in single crystalline samples to $\simeq 15\,\mu\Omega$ cm[9,40] in polycrystalline samples. Also, the switching field of our sample $H_c = 76$ mT is of the same order of magnitude as the one obtained earlier in similar conditions.[18]

The high aspect ratio of NW (1:60) allows one to characterize switching using analytical estimations for magnetization reversal in an infinite cylinder. The magnetization of the infinite cylinder of a diameter d above critical diameter $d_0 = 5.2 l_e \simeq 42$ nm[18,42] reverses via a curling mode at the coercive field[18]

$$H_c = \frac{M_s}{2} \frac{a(a+1)}{\sqrt{a^2 + (1+2a)\cos^2 \theta}}, \qquad (5)$$

where $a = 1.08(d_0/d)^2$ and θ is the angle between the nanowire axis and the external magnetic field.[24] In the present experiment, $\theta = 0$ and $a = 0.1$, implying $H_c = M_s a/2 \approx 34$ mT. The estimated coercive field is smaller by a factor of 2.3 than the experimental one indicating a crucial role of polycrystalline morphology on the magnetization reversal process.

MR behavior of ferromagnetic NWs can be studied numerically with micromagnetic simulations, where Eq. (4) is the basis for micromagnetic representation of MR as it was proposed in Ref. 43. As a first step, we solve Eq. (1) to obtain a macrospin function $\vec{m}(x, y, z, \vec{H})$. Next, every simulation cell is assumed as a mono-domain particle [Eq. (4)] and the total resistance is computed averaging resistances in cross-sections (y, z) for every x_i and then summarizing them as resistances in series. Commonly, parameters ρ_o and β in Eq. (4) are used as fitting parameters or are derived from the experiment.

First, we simulate magnetization reversal and LMR for the "ideally soft" Ni NW at the magnetic field aligned with its axis. The NW is represented by a cuboid of size $4000 \times 132 \times 132$ nm^3 (see Fig. 3). Smaller cross-section is used in order to exclude nonmagnetic 2–4 nm thick nickel oxide coating. The cuboid NW is meshed with cells $2 \times 6 \times 6$ nm^3 below l_e. Simulated hysteresis loop $m_x(H)$ of the "ideally soft" Ni NW is shown in Fig. 4 (blue curve). The coercive field of the simulated "ideally soft" NW $H_c = 31$ mT matches well the estimated analytical value indicating the applicability of micromagnetic simulations. The fit of the experimental LMR curve employing the hysteresis loop and Eq. (4) yields $\rho_0^{fit} = 7.57\,\mu\Omega$ cm, $\beta^{fit} = 5\%$ and is shown in Fig. 2 (blue curve).

We associate the discrepancy between simulated and experimental LMR curves with a polycrystalline nature of the synthesized NW [Fig. 1(b)], where every crystallite possesses cubic magnetocrystalline anisotropy that contributed to $\mathbf{H}_{eff}$ with $\mathbf{H}_a$ in Eqs. (1) and (2). We account the polycrystalline nature of the nanowire dividing the cuboid into grains using voronoi tessellation (see Fig. 3), following Refs. 44 and 45.
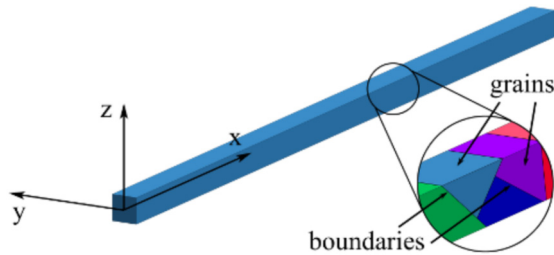
FIG. 3. Schematic illustration of the micromagnetic simulated NW. The NW is represented by a cuboid. The polycrystalline structure of the NW is represented by dividing the cuboid into grains using voronoi tessellation and by assigning random crystallographic orientation of Ni cubic magnetocrystalline anisotropy to each grain. The role of grain boundaries is represented by uniaxial anisotropy at intergrain areas aligned normally to intergrain surfaces.

The average size of the cuboid cross-section is equal to the diameter of the NW. Since diffraction analysis [Fig. 1(a)] showed no preferred orientation of crystallites, we set the orientation of the orthonormal basis of crystallographic axes ($\mathbf{u}_1$, $\mathbf{u}_2$, $\mathbf{u}_3$) for each grain randomly. This approach is referred to commonly as the random anisotropy model.[46,47] The following parameters of the cubic magnetocrystalline anisotropy were used for simulations:[48] $K_1 = 126.3 \times 10^3$ J/m^3 and $K_2 = 57.8 \times 10^3$ J/m^3. The green curve in Fig. 4 shows the simulated hysteresis loop $m_x(H)$ of the grained Ni NW. The fit of the experimental LMR curve using the hysteresis loop of the grained NW yields $\rho_0^{\text{fit}} = 7.73\,\mu\Omega$ cm, $\beta^{\text{fit}} = 3\%$ (green curve in Fig. 2). Coercive field $H_c = 50$ mT is substantially larger than the one obtained for the "ideally soft" NW confirming the influence of polycrystalline morphology on the NW in magnetization reversal.

The simulated H_c of grained NW still remains smaller than the experimental value by a factor of 1.5. The remaining discrepancy between the experimental and simulated LMR
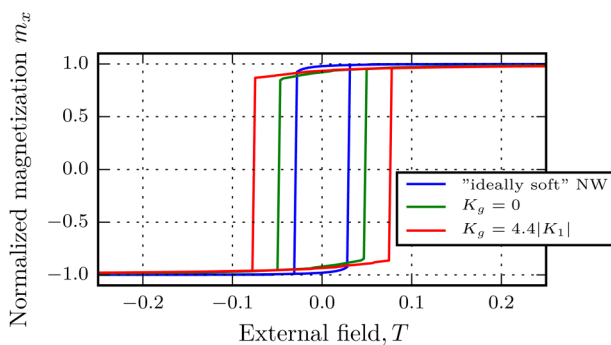
curves is associated with the influence of intergrain surfaces, i.e., grain boundaries, on the magnetization reversal process. Indeed, the crystal structure at grain boundaries is broken and magnetic properties of the boundaries should differ from those of the crystal. With micromagnetic simulations, grain boundaries can be considered as areas with effective grain boundary anisotropy or effective intergrain exchange coupling.[28,29] Keeping the grained structure of the NW, we assign uniaxial anisotropy to micromagnetic cells at grain boundaries with the parameter of uniaxial anisotropy K_g and the axis of uniaxial anisotropy aligned perpendicular to the intergrain surface (Fig. 3).

The actual value of K_g is unknown. In order to determine K_g, we simulated a set of hysteresis loops at different K_g and derived the dependence of the coercive field on K_g (see Fig. 5). At $K_g/|K_1| \simeq 4.4$, the simulated coercive field corresponds exactly to the experimental $H_c = 76$ mT.

We should note that in this work, we have measured a set of samples that were made by the same technique in the same geometry but with different diameters in a range from 100 to 150 nm. The estimated parameter K_g for each sample was in a narrow range 4–5 $|K_1|$. A slight variation of K_g for different samples can be explained by a marginal variation of the magnetic properties of grain boundaries for different NWs.

The hysteresis loop $m_x(H)$ calculated with $K_g/|K_1| \simeq 4.4$ is shown in Fig. 4 with a red curve. The fit of experimental LMR (red curve in Fig. 2) shows a good match with experimental data and yields $\rho_0^{\text{fit}} = 7.69\,\mu\Omega$ cm, $\beta^{\text{fit}} = 4\%$. Note that the resistivity ρ_0 obtained from fitting the LMR corresponds to measured resistivity $\rho = 7.7\,\mu\Omega$ cm at temperature $T = 10$ K. Thus, we confirm the crucial role of polycrystalline morphology of the studied nanowire for LMR, where magnetocrystalline anisotropy of randomly oriented grains and effective uniaxial anisotropy at grain boundaries play an equally substantial role.

As the final comment, we discuss the influence of effective uniaxial anisotropy at grain boundaries on the magnetization reversal process. The plot $H_c(K_g)$ in Fig. 5 can be divided into three distinct ranges indicated with dashed lines.
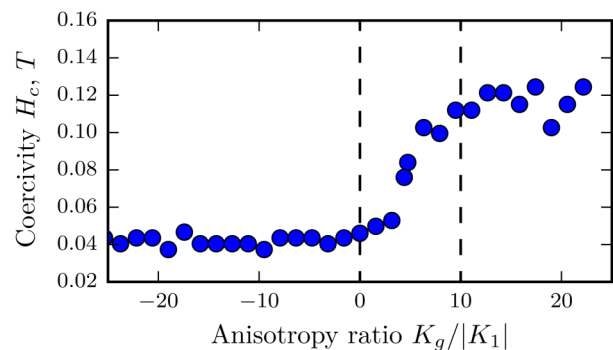

FIG. 4. Simulated hysteresis loops $m_x(H)$ calculated for the "ideally soft" crystal (blue curve), for polycrystalline NW with randomly oriented grains (green curve), and for polycrystalline NW with randomly oriented grains and effective uniaxial anisotropy at grain boundaries (red curve, $K_g \simeq 4.4|K_1|$).

FIG. 5. Dependence of the coercive field of polycrystalline NW on the parameter of uniaxial anisotropy at the grain boundary $H_c(K_g)$. The experimental value of coercive field $H_c = 76$ mT corresponds to $K_g/|K_1| \simeq 4.4$.

At $K_g < 0$, magnetization reversal occurs via the curling mode when upon demagnetization, vortices are formed at the edges of the NW and propagate toward each other. In this case, the actual properties of the edges do not affect magnetostatics of vortex formation and propagation, coercive field $H_c \approx 40$ mT depends on K_g marginally. At large values, $K_g > 10|K_1|$, effective anisotropy of grain boundaries dominates the magnetization reversal process and prevents formation and propagation of the vortex. The origin of the scatter at these values is due to the lack of averaging over grains on the length of the nanowire. In our model, the grain size is the diameter of the nanowire as it is in the experiment. There are about 40 grains in the modeled wire. Thus, different parts of grains play a different role in vortex pinning in magnetization reversal processes at different Kg values. If there were smaller grains, then this pinning effect would be averaged over the nanowire length and Fig. 5 would be smoother.

At the intermediate transition range $0 < K_g < 10|K_1|$, the coercive field shows a strong dependence on K_g. In this range, the magnetization reversal occurs via the curling mode, as at $K_g < 10|K_1|$, yet the vortices experience pinning on grain boundaries upon propagation. Thus, high H_c of the Ni NW in this work is accounted for by curling-mode magnetization reversal when the vortices are formed and propagate in a randomly oriented grain structure of the NW and propagation is inhibited at grain boundaries.

V. CONCLUSION

In conclusion, in this work, we studied the magnetoresistance of an individual polycrystalline nickel nanowire at low temperature. The longitudinal magnetoresistance measurements have indicated a low resistivity and a large coercive field of the Ni NW with a diameter of 137 nm. Micromagnetic simulations have shown that large $H_c = 76$ mT is accounted for by the polycrystalline structure of the studied nanowire where both magnetocrystalline anisotropy of randomly oriented grains and effective uniaxial anisotropy at the grain boundaries contribute to the enhanced H_c as compared to the ideal structure. Magnetization reversal occurs via the curling mode when the vortices are formed and propagate in the NW and propagation is inhibited at grain boundaries. The applicability of micromagnetic simulations is confirmed by an agreement between experiment and simulated MR curves.

REFERENCES

[1]H. Pan, B. Liu, J. Yi, C. Poh, S. Lim, J. Ding, Y. Feng, C. Huan, and J. Lin, J. Phys. Chem. B **109**, 3094 (2005).

[2]C. Yu, Y. Yu, H. Sun, T. Xu, X. Li, W. Li, Z. Gao, and X. Zhang, Mater. Lett. **61**, 1859 (2007).

[3]S. Zhang, W. Gan, J. Kwon, F. Luo, G. Lim, J. Wang, and W. Lew, Sci. Rep. **6**, 24804 (2016).

[4]K. Nielsch, R. Wehrspohn, J. Barthel, J. Kirschner, U. Gösele, S. Fischer, and H. Kronmüller, Appl. Phys. Lett. **79**, 1360 (2001).

[5]M. Hayashi, L. Thomas, R. Moriya, C. Rettner, and S. S. Parkin, Science **320**, 209 (2008).

[6]R. Verba, M. Carpentieri, G. Finocchio, V. Tiberkevich, and A. Slavin, Sci. Rep. **6**, 25018 (2016).

[7]M. Alnassar, A. Alfadhel, Y. P. Ivanov, and J. Kosel, J. Appl. Phys. **117**, 17D711 (2015).

[8]P. D. McGary, L. Tan, J. Zou, B. J. Stadler, P. R. Downey, and A. B. Flatau, J. Appl. Phys. **99**, 08B310 (2006).

[9]J. Wang, M. Singh, M. Tian, N. Kumar, B. Liu, C. Shi, J. Jain, N. Samarth, T. Mallouk, and M. Chan, Nat. Phys. **6**, 389 (2010).

[10]M. Kompaniiets, O. Dobrovolskiy, C. Neetzel, E. Begun, F. Porrati, W. Ensinger, and M. Huth, J. Appl. Phys. **116**, 073906 (2014).

[11]O. V. Skryabina, S. N. Kozlov, S. V. Egorov, A. A. Klimenko, V. V. Ryazanov, S. V. Bakurskiy, M. Y. Kupriyanov, N. V. Klenov, I. I. Soloviev, A. A. Golubov, K. S. Napolskii, I. A. Golovchansky, and V. S. Stolyarov, "Anomalous magneto-resistance of Ni-nanowire / Nb hybrid system" (to be published).

[12]X. Zhang, Y. Zhou, M. Ezawa, G. Zhao, and W. Zhao, Sci. Rep. **5**, 11369 (2015).

[13]M. Charilaou, H.-B. Braun, and J. F. Löffler, Phys. Rev. Lett. **121**, 097202 (2018).

[14]J. Escrig, D. Altbir, M. Jaafar, D. Navas, A. Asenjo, and M. Vázquez, Phys. Rev. B **75**, 184429 (2007).

[15]D. Sellmyer, M. Zheng, and R. Skomski, J. Phys. Condens. Matter **13**, R433 (2001).

[16]K. Napolskii, A. Eliseev, N. Yesin, A. Lukashin, Y. D. Tretyakov, N. Grigorieva, S. Grigoriev, and H. Eckerlebe, Physica E **37**, 178 (2007).

[17]V. Vega, T. Böhnert, S. Martens, M. Waleczek, J. M. Montero-Moreno, D. Görlitz, V. Prida, and K. Nielsch, Nanotechnology **23**, 465709 (2012).

[18]W. Wernsdorfer, B. Doudin, D. Mailly, K. Hasselbach, A. Benoit, J. Meier, J.-P. Ansermet, and B. Barbara, Phys. Rev. Lett. **77**, 1873 (1996).

[19]R. Ferre, K. Ounadjela, J. George, L. Piraux, and S. Dubois, Phys. Rev. B **56**, 14066 (1997).

[20]Y. Rheem, B. Yoo, W. Beyermann, and N. Myung, Nanotechnology **18**, 015202 (2006).

[21]M. V. Kamalakar and A. Raychaudhuri, Phys. Rev. B **79**, 205417 (2009).

[22]M. V. Kamalakar, A. Raychaudhuri, X. Wei, J. Teng, and P. D. Prewett, Appl. Phys. Lett. **95**, 013112 (2009).

[23]E. Frei, S. Shtrikman, and D. Treves, Phys. Rev. **106**, 446 (1957).

[24]S. Shtrikman and D. Treves, J. Phys. Radium **20**, 286 (1959).

[25]A. Arrott, B. Heinrich, and A. Aharoni, IEEE Trans. Magn. **15**, 1228 (1979).

[26]G. Herzer, *Properties and Applications of Nanocrystalline Alloys from Amorphous Precursors* (Springer, 2005), pp. 15–34.

[27]C. França, Y. Guerra, D. Valadão, J. Holanda, and E. Padrón-Hernández, Comput. Mater. Sci. **128**, 42 (2017).

[28]Q. Bian and M. Niewczas, J. Appl. Phys. **116**, 033921 (2014).

[29]Q. Bian and M. Niewczas, J. Appl. Phys. **117**, 013909 (2015).

[30]C.-L. Xu, H. Li, G.-Y. Zhao, and H.-L. Li, Mater. Lett. **60**, 2335 (2006).

[31]K. S. Napolskii, I. V. Roslyakov, A. A. Eliseev, D. I. Petukhov, A. V. Lukashin, S.-F. Chen, C.-P. Liu, and G. A. Tsirlina, Electrochim. Acta **56**, 2378 (2011).

[32]O. V. Skryabina, S. V. Egorov, A. S. Goncharova, A. A. Klimenko, S. N. Kozlov, V. V. Ryazanov, S. V. Bakurskiy, M. Y. Kupriyanov, A. A. Golubov, K. S. Napolskii, and V. S. Stolyarov, Appl. Phys. Lett. **110**, 222605 (2017).

[33]H. Corte-León, V. Nabaei, A. Manzin, J. Fletcher, P. Krzysteczko, H. W. Schumacher, and O. Kazakova, Sci. Rep. **4**, 6045 (2014).

[34]J. E. Miltat and M. J. Donahue, *Handbook of Magnetism and Advanced Magnetic Materials* (Wiley, 2007).

[35]A. Vansteenkiste, J. Leliaert, M. Dvornik, M. Helsen, F. Garcia-Sanchez, B. Van Waeyenberge, AIP Adv. **4**, 107133 (2014).

[36]B. Yoo, Y. Rheem, W. P. Beyermann, and N. V. Myung, Nanotechnology **17**, 2512 (2006).

[37]Y. Rheem, B. Yoo, W. Beyermann, and N. Myung, Nanotechnology **18**, 125204 (2007).

[38]J. Wegrowe, D. Kelly, A. Franck, S. Gilbert, and J.-P. Ansermet, Phys. Rev. Lett. **82**, 3681 (1999).

[39]T. McGuire and R. Potter, IEEE Trans. Magn. **11**, 1018 (1975).

[40]M. Ou, T. Yang, S. Harutyunyan, Y. Chen, C. Chen, and S. Lai, Appl. Phys. Lett. **92**, 063101 (2008).

[41]T. Böhnert, V. Vega, A.-K. Michel, V. M. Prida, and K. Nielsch, Appl. Phys. Lett. **103**, 092407 (2013).

[42]R. Hertel and J. Kirschner, Physica B **343**, 206 (2004).

[43]R. A. Silva, T. S. Machado, G. Cernicchiaro, A. P. Guimarães, and L. C. Sampaio, Phys. Rev. B **79**, 134434 (2009).

[44]J. Lau, R. McMichael, and M. Donahue, J. Res. Natl. Inst. Stand. Technol. **114**, 57 (2009).

[45]J. Leliaert, B. Van de Wiele, A. Vansteenkiste, L. Laurson, G. Durin, L. Dupré, B. Van Waeyenberge, J. Appl. Phys. **115**, 233903 (2014).

[46]J. Fidler and T. Schref, J. Phys. D Appl. Phys. **33**, R135 (2000).

[47]I. Golovchanskiy, V. Bol'ginov, V. Stolyarov, N. Abramov, A. B. Hamida, O. Emelyanova, B. Stolyarov, M. Y. Kupriyanov, A. Golubov, and V. Ryazanov, Phys. Rev. B **94**, 214514 (2016).

[48]M. Getzlaff, *Fundamentals of Magnetism* (Springer Science & Business Media, 2007).